

# A hierarchical carbon nanofiber-In<sub>2</sub>S<sub>3</sub> photocatalyst with well controlled nanostructures for highly efficient hydrogen production under visible light

Peng Gao<sup>\*</sup>, Anran Li<sup>\*\*</sup>, Minghang Tai<sup>\*</sup>, Zhaoyang Liu<sup>\*</sup>, and Darren Sun<sup>\*</sup>

<sup>\*</sup> School of Civil and Environmental Engineering, Nanyang Technological University, Singapore,

<sup>\*\*</sup> School of Materials and Science Engineering, Nanyang Technological University, Singapore

## ABSTRACT

In this study, a novel hierarchical visible-light responsive photocatalyst was delicately designed and synthesized by anchoring In<sub>2</sub>S<sub>3</sub> flower-like nanostructures on non-woven carbon nanofibers (CNF) for the first time. The nanostructures of these CNF-In<sub>2</sub>S<sub>3</sub> composites were fine tuned, with the aim to achieve the highest photocatalytic hydrogen production activity under visible light. The results indicated that the hierarchical CNF-In<sub>2</sub>S<sub>3</sub>-24h photocatalyst exhibited exceptionally high hydrogen evolution rate (ca. 390 μmol h<sup>-1</sup>), which was around 15 and 12 times higher than that of pure In<sub>2</sub>S<sub>3</sub> and commercial N-TiO<sub>2</sub> nanoparticles, respectively. The prominent photocatalytic hydrogen production activity of the hierarchical CNF-In<sub>2</sub>S<sub>3</sub>-24h photocatalyst can be attributed to the excellent properties of enhanced light absorption and efficient charge separation, which are all derived from the special 3D hierarchical nanostructures.

**Keywords:** hierarchical, nanostructure, composite, photocatalyst, hydrogen

## 1 INTRODUCTION

The excessive consumption of fossil fuels (petroleum, coal and natural gas) leading to the energy crisis and global warming have impelled the researchers to search for other renewable clean energy [1]. Hydrogen as a renewable clean energy has attracted a lot attention because of its high heat conversion efficiency and zero carbon emission [2]. In the last several decades, the photocatalytic hydrogen production had attracted enormous research interests, since the first report was published by Fujishima and Honda on the photo-electrochemical water splitting by an n-type TiO<sub>2</sub> electrode [3]. Recently, the visible-light responsive photocatalysts, such as In<sub>2</sub>S<sub>3</sub>, have been considered to be promising candidates for hydrogen production due to their ability of using the majority of solar light [4]. For example, Chai et al. synthesized In<sub>2</sub>S<sub>3</sub>/(Pt-TiO<sub>2</sub>) photocatalyst through a multi-step method and investigated its hydrogen evolution activity under visible light [5]. However, the hydrogen production activity of reported In<sub>2</sub>S<sub>3</sub> is not high. In recent years, combination of photocatalysts with carbon materials, and controlled synthesis of hierarchical photocatalysts with special nanostructures have been demonstrated to be two promising approaches to improve

the performance of the photocatalysts [6]. Hence, in this study, the novel hierarchical visible-light responsive CNF-In<sub>2</sub>S<sub>3</sub> composites with tunable morphology was controlled synthesized *via* a one-pot hydrothermal reaction for photocatalytic hydrogen production for the first time. Three kinds of CNF-In<sub>2</sub>S<sub>3</sub> nanostructures, including CNF-In<sub>2</sub>S<sub>3</sub>-8h, CNF-In<sub>2</sub>S<sub>3</sub>-16h and CNF-In<sub>2</sub>S<sub>3</sub>-24h, were delicately prepared by adjusting the reaction time. The formation mechanism of these hierarchical nanostructures was proposed by investigation of the morphology evolution process through FESEM characterization. The hierarchical CNF-In<sub>2</sub>S<sub>3</sub>-24h photocatalyst shows the highest hydrogen evolution rate among all investigated samples, including CNF-In<sub>2</sub>S<sub>3</sub>-8h, CNF-In<sub>2</sub>S<sub>3</sub>-16h, pure In<sub>2</sub>S<sub>3</sub> and commercial N-TiO<sub>2</sub> nanoparticles. Hence, this study opens up a new avenue for controlled synthesis of hierarchical carbon related nanostructures which can be good candidates in clean energy production field.

## 2 MATERIALS AND METHODS

### Materials

L-cysteine, tetraethylorthosilicate (TEOS), Indium chloride tetrahydrate (InCl<sub>3</sub> 4H<sub>2</sub>O, 99.99%), acetic acid (HAC), polyacrylonitrile (PAN, MW=150000 g/mol), and sodium hydroxide (NaOH) were obtained from Sigma-Aldrich. Dimethyl formamide (DMF) was purchased from Merck Ltd. All chemicals were used as received without further purification. Deionized (DI) water was produced from Millipore Milli-Q water purification system.

### Synthesis of CNF-In<sub>2</sub>S<sub>3</sub> composites

CNF-In<sub>2</sub>S<sub>3</sub> composites, including CNF-In<sub>2</sub>S<sub>3</sub>-8h, CNF-In<sub>2</sub>S<sub>3</sub>-16h and CNF-In<sub>2</sub>S<sub>3</sub>-24h, were synthesized by the one-pot hydrothermal method [7]. In a typical process, 710 mg (2 mmol) L-cysteine and 445 mg (1.5 mmol) InCl<sub>3</sub> 4H<sub>2</sub>O were dissolved in 90 mL DI water. Subsequently, the pH of the solution was adjusted to 8 by adding 1 mol/L NaOH solution. Then, 200 mg of CNF was added into the mixed solvent and ultrasonicated for 30 min. Finally, the mixture was transferred into a 125 mL Teflon-lined stainless autoclave and kept at 180 °C for 24 h. The prepared product was washed with ethanol and DI water for three times, respectively. The hydrothermal time was controlled to be 8h, 16h and 24h in order to get CNF-In<sub>2</sub>S<sub>3</sub>-8h, CNF-In<sub>2</sub>S<sub>3</sub>-16h and CNF-In<sub>2</sub>S<sub>3</sub>-24h composites, individually. As comparison, pure In<sub>2</sub>S<sub>3</sub> was synthesized under the same condition without addition of CNF.

## Characterization

The morphology of CNF-In<sub>2</sub>S<sub>3</sub> composites, including CNF-In<sub>2</sub>S<sub>3</sub>-8h, CNF-In<sub>2</sub>S<sub>3</sub>-16h and CNF-In<sub>2</sub>S<sub>3</sub>-24h, was investigated by field emission scanning electron microscopy (FESEM, JSM-7600F). In addition, the microstructure of CNF-In<sub>2</sub>S<sub>3</sub>-24h composites was evaluated by transmission electron microscopy (TEM, JEOL 2010-H microscope) operating at 200 kV. Furthermore, UV-visible (UV-Vis) spectra of pure In<sub>2</sub>S<sub>3</sub> and CNF-In<sub>2</sub>S<sub>3</sub>-24h composites were investigated by the UV-visible spectrometer (UV-visible resource 3000). Photoluminescence (PL) spectra of pure In<sub>2</sub>S<sub>3</sub> and CNF-In<sub>2</sub>S<sub>3</sub>-24h composites were measured on the spectrofluorophotometer (Shimadzu RF-5301) with an excitation wavelength of 420 nm.

## Photocatalytic hydrogen production

The hydrogen evolution reaction was performed in a three-necked Pyrex flask (volume: 100 ml) with the three openings of the flask sealed by silicone rubber. A 350 W Xe arc lamp were used as visible light source and put 2 cm beside the flask. To keep a constant reaction temperature of 25 °C, the flask was cooled by water under the bottom. 50 mg of powdered photocatalysts, including In<sub>2</sub>S<sub>3</sub>, CNF-In<sub>2</sub>S<sub>3</sub>-24h composites, and N-TiO<sub>2</sub>, were well suspended in 10 volume% methanol/water mixture. Hydrogen produced from the photocatalytic process was collected by a water displacement gas trap, from which the volume of the evolved hydrogen was measured.

## 3 RESULTS AND DISCUSSION

The surface morphology of CNF-In<sub>2</sub>S<sub>3</sub> composites with different hydrothermal reaction time (8h, 16h and 24h) was thoroughly investigated by FESEM characterization, in order to study the formation process of the hierarchical CNF-In<sub>2</sub>S<sub>3</sub> composites. Figure 1a-f show the FESEM images of CNF-In<sub>2</sub>S<sub>3</sub>-8h, CNF-In<sub>2</sub>S<sub>3</sub>-16h, and CNF-In<sub>2</sub>S<sub>3</sub>-24h, respectively. Figure 1a and b are FESEM images of CNF-In<sub>2</sub>S<sub>3</sub>-8h composites. Small and sparse In<sub>2</sub>S<sub>3</sub> nanosheets can be clearly observed on the surface of CNF, as seen in Figure 1a and b. In addition, it should be noted that no flower-like nanostructures can be found at current stage. The size and number of In<sub>2</sub>S<sub>3</sub> nanostructures were significantly increased when the reaction time was further increased to 16h (CNF-In<sub>2</sub>S<sub>3</sub>-16h), as shown in Figure 1c and d. Moreover, Figure 1d shows that some In<sub>2</sub>S<sub>3</sub> nanosheets were assembled together to form flower-like nanostructures. When the hydrothermal reaction time was lengthened to 24h, the secondary In<sub>2</sub>S<sub>3</sub> flower-like nanostructures were completely formed on the surface of CNF, as shown in Figure 1e and f. Figure 1e and f show that In<sub>2</sub>S<sub>3</sub> flower-like nanostructures are uniformly assembled on all CNF instead of randomly deposited on CNF, indicating that this one-pot hydrothermal approach is highly efficient to controlled synthesis of CNF based hierarchical nanostructures. In addition, the size of individual In<sub>2</sub>S<sub>3</sub> flower-like nanostructure is around 500 nm.

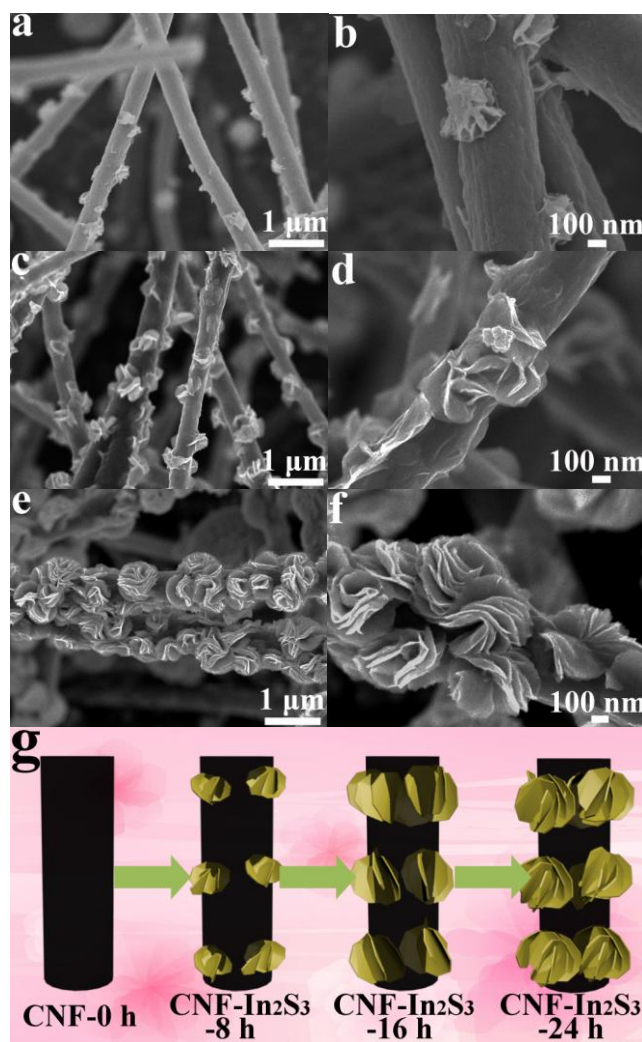


Figure 1: (a) and (b) FESEM images of CNF-In<sub>2</sub>S<sub>3</sub>-8h composites; (c) and (d) FESEM images of CNF-In<sub>2</sub>S<sub>3</sub>-16h composites; (e) and (f) FESEM images of CNF-In<sub>2</sub>S<sub>3</sub>-24h composites; and (g) schematic illustration of formation process of CNF-In<sub>2</sub>S<sub>3</sub>-24h composites.

The hierarchical flower-like nanostructures are beneficial for light scattering and absorption, which can further improve the photocatalytic performance [8]. Hence, by investigation of the morphology of CNF-In<sub>2</sub>S<sub>3</sub> composites at different intervals of reaction time, a tentative mechanism for the formation of CNF-In<sub>2</sub>S<sub>3</sub>-24h composites has been schematically proposed in Figure 1g. In these experiments, firstly, the In<sup>3+</sup> and S<sup>2-</sup> start to adsorb and nucleate on the surface of CNF to form the sparse and small In<sub>2</sub>S<sub>3</sub> nanosheets, labeled as CNF-In<sub>2</sub>S<sub>3</sub>-8h. Subsequently, the initial formed In<sub>2</sub>S<sub>3</sub> nanosheets continue to grow larger and assemble together to form the secondary In<sub>2</sub>S<sub>3</sub> flower-like nanostructures by consumption of the precursors (In<sup>3+</sup> and S<sup>2-</sup>), marked as CNF-In<sub>2</sub>S<sub>3</sub>-16h. At the final stage, the hierarchical CNF-In<sub>2</sub>S<sub>3</sub>-24h composites are prepared, which are composed of numerous flower-like In<sub>2</sub>S<sub>3</sub> nanostructures surrounding on the surface of CNF.

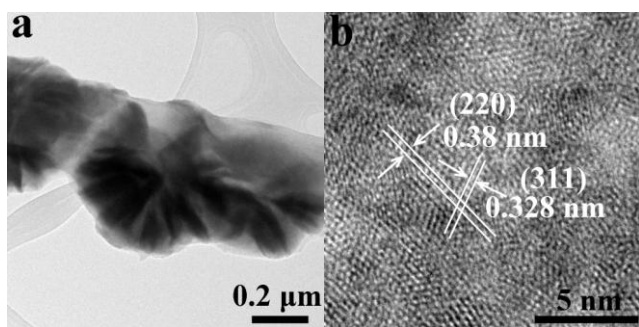


Figure 2: (a) TEM image of CNF-In<sub>2</sub>S<sub>3</sub>-24h composites; and (b) HRTEM image of CNF-In<sub>2</sub>S<sub>3</sub>-24h composites.

Figure 2a and b are TEM and HRTEM images of the hierarchical CNF-In<sub>2</sub>S<sub>3</sub>-24h composites, respectively. Figure 2a exhibits that several flower-like In<sub>2</sub>S<sub>3</sub> nanostructures are uniformly assembled on the surface of CNF. In addition, the diameters of individual flower-like In<sub>2</sub>S<sub>3</sub> nanostructure and CNF are about 480 nm and 360 nm, respectively, which are coordinated well with the results of FESEM analyses. Figure 2b shows the HRTEM image of CNF-In<sub>2</sub>S<sub>3</sub>-24h, which is taken from the edge of one flower-like In<sub>2</sub>S<sub>3</sub> nanostructure. The two distinctive lattice fringes of 0.38 nm and 0.328 nm can be assigned to the (220) and (311) facets of cubic β-In<sub>2</sub>S<sub>3</sub>, individually [9]. The clear lattice fringes indicate the good crystallinity of the flower-like In<sub>2</sub>S<sub>3</sub> nanostructures. It should be noted that the good crystallinity of the photocatalysts can reduce the charge recombination rate, which can enhance the photocatalytic activity. Hence, the results of FESEM and TEM characterization demonstrate that CNF-In<sub>2</sub>S<sub>3</sub> composites have been successfully prepared.

The photocatalytic hydrogen production activities of In<sub>2</sub>S<sub>3</sub>, CNF-In<sub>2</sub>S<sub>3</sub>-24h composites, and N-TiO<sub>2</sub> have been thoroughly investigated to find out the advantages of CNF-In<sub>2</sub>S<sub>3</sub>-24h. Figure 3a shows that CNF-In<sub>2</sub>S<sub>3</sub>-24h composites produce about 1550 μmol of H<sub>2</sub> within 4h, which is much higher than that of pure In<sub>2</sub>S<sub>3</sub> (ca. 105 μmol) and N-TiO<sub>2</sub> (ca. 133 μmol). The low hydrogen evolution efficiency of pure In<sub>2</sub>S<sub>3</sub> and N-TiO<sub>2</sub> can be attributed to the fast charge recombination rate which reduces the life-time of photo-generated electrons. The hydrogen evolution efficiency was increased significantly after the introduction of CNF because CNF is a good electron accumulator which can improve the efficiency of charge separation. The detailed mechanism will be discussed in the following part. The average hydrogen evolution rate of CNF-In<sub>2</sub>S<sub>3</sub>-24h is around 390 μmol h<sup>-1</sup>, which is about 15 and 12 times higher than that of pure In<sub>2</sub>S<sub>3</sub> (ca. 26 μmol h<sup>-1</sup>) and commercial N-TiO<sub>2</sub> nanoparticles (ca. 33 μmol h<sup>-1</sup>), respectively, as shown in Figure 3b.

The outstanding photocatalytic hydrogen production activity of CNF-In<sub>2</sub>S<sub>3</sub>-24h composites can be attributed to the following two factors, including enhanced light absorption and scattering, and anti-recombination of photo-

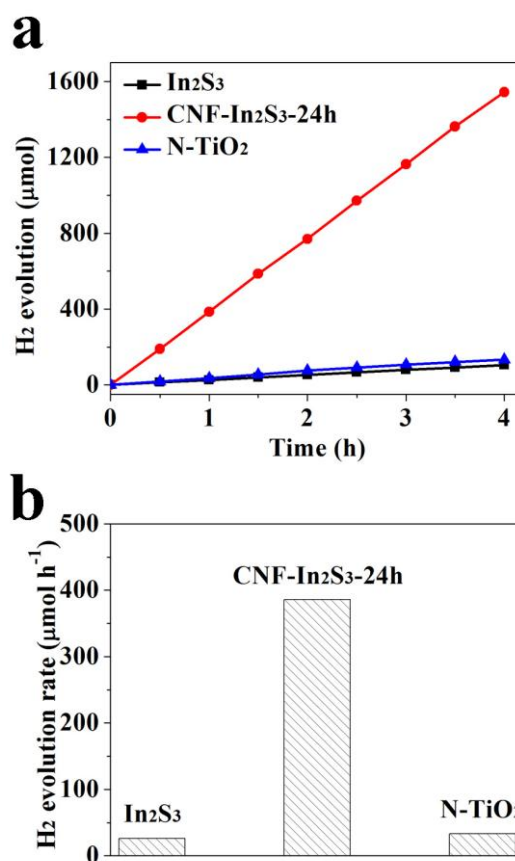


Figure 3: (a) Photocatalytic hydrogen evolution activity of In<sub>2</sub>S<sub>3</sub>, CNF-In<sub>2</sub>S<sub>3</sub>-24h composites, and N-TiO<sub>2</sub>; and (b) Average hydrogen evolution rate of In<sub>2</sub>S<sub>3</sub>, CNF-In<sub>2</sub>S<sub>3</sub>-24h composites, and N-TiO<sub>2</sub>.

generated electrons and holes. Figure 4a shows the UV-Vis absorption spectra of pure In<sub>2</sub>S<sub>3</sub> and CNF-In<sub>2</sub>S<sub>3</sub>-24h composites. The absorption edges of In<sub>2</sub>S<sub>3</sub> and CNF-In<sub>2</sub>S<sub>3</sub>-24h are both located at around 600 nm, which is in the visible light region. Remarkably, CNF-In<sub>2</sub>S<sub>3</sub>-24h composites show a much stronger absorption in the whole visible light region (from 600 nm to 800 nm) than that of In<sub>2</sub>S<sub>3</sub> because of the introduction of CNF. In addition, no shift in the absorption edge of CNF-In<sub>2</sub>S<sub>3</sub>-24h composites can be found, indicating that carbon species do not dope into the lattice of In<sub>2</sub>S<sub>3</sub> sheets. According to the Kubelka-Munk function, the bandgaps of In<sub>2</sub>S<sub>3</sub> and CNF-In<sub>2</sub>S<sub>3</sub>-24h composites are calculated to be around 2.1 eV, as shown in the inset of Figure 4a [10]. The charge separation activity was investigated by PL measurement, as shown in Figure 4b. The intensity of PL spectra indicates the charge recombination rate. Hence, the PL measurement is a powerful technique in the investigation of the photocatalysts. Figure 4b shows the intensity of pure In<sub>2</sub>S<sub>3</sub> is greatly higher than that of CNF-In<sub>2</sub>S<sub>3</sub>-24h composites. The results of PL spectra demonstrate that the charge

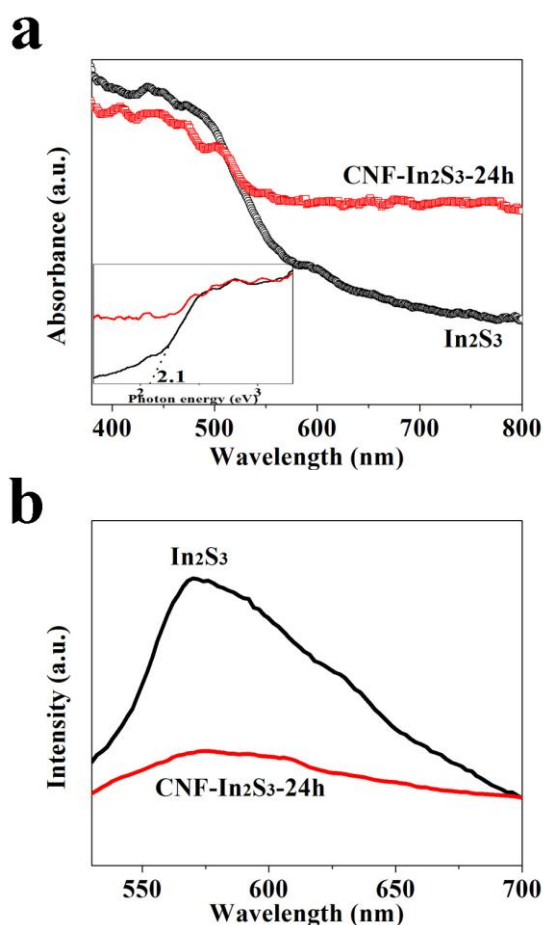


Figure 4: (a) UV-Vis spectra of pure  $\text{In}_2\text{S}_3$  and CNF- $\text{In}_2\text{S}_3$ -24h composites (inset: the corresponding Kubelka-Munk-transformed reflection spectra); and (b) PL spectra of pure  $\text{In}_2\text{S}_3$  and CNF- $\text{In}_2\text{S}_3$ -24h composites.

recombination rate of CNF- $\text{In}_2\text{S}_3$ -24h composites have been significantly suppressed after introducing CNF into the photocatalytic system. The above results confirm that efficient light absorption ability and suppressed charge recombination rate are two essential factors governing the photocatalytic hydrogen production activity.

A tentative hydrogen production mechanism has been proposed and schematically illustrated in Figure 5. Generally, the hierarchical nanostructure of CNF- $\text{In}_2\text{S}_3$ -24h composites is favorable for light scattering and reflection, which enhances the light utilization rate (confirmed by Figure 4a). In the first step, the electron-hole pairs of  $\text{In}_2\text{S}_3$  are generated under visible light irradiation, and the photo-generated electrons jump from the valance band (VB) to the conduction band (CB) of  $\text{In}_2\text{S}_3$ , as shown in the right side of Figure 5. Subsequently, the photo-generated electrons in the CB of  $\text{In}_2\text{S}_3$  transfer immediately to the adjacent surface of CNF, while leaving the photo-generated holes in the VB of  $\text{In}_2\text{S}_3$ . This charge separation process reduces the recombination rate of electron-hole pairs, which further improves the hydrogen production efficiency. Finally, the

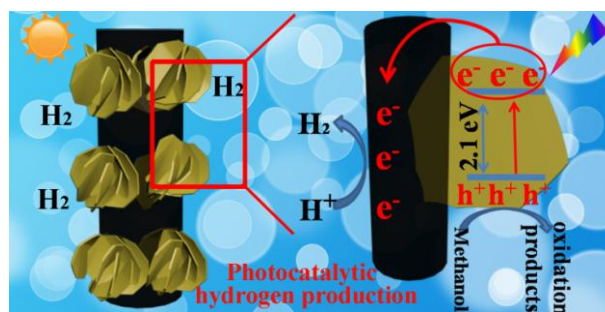


Figure 5: Schematic illustration of mechanism of photocatalytic hydrogen production process in the system of CNF- $\text{In}_2\text{S}_3$ -24h composites.

photo-generated electrons react with the protons ( $\text{H}^+$ ) to produce hydrogen.

## 4 CONCLUSION

In summary, the hierarchical CNF- $\text{In}_2\text{S}_3$  composites, including CNF- $\text{In}_2\text{S}_3$ -8h, CNF- $\text{In}_2\text{S}_3$ -16h and CNF- $\text{In}_2\text{S}_3$ -24h, have been controlled synthesized by one-pot hydrothermal method. The morphology and microstructure of CNF- $\text{In}_2\text{S}_3$  composites have been investigated thoroughly. The results show that photocatalytic hydrogen production efficiency of CNF- $\text{In}_2\text{S}_3$ -24h is significantly higher than that of pure  $\text{In}_2\text{S}_3$  and commercial N- $\text{TiO}_2$ , which can be attributed to the excellent light absorption and enhanced charge separation properties.

## REFERENCES.

- [1] E. Chornet, S. Czernik, Nature, 418, 928-929, 2002.
- [2] J. Ng, S. Xu, X. Zhang, H.Y. Yang, D.D. Sun, Adv. Funct. Mater., 20, 4287-4294, 2010.
- [3] A. Fujishima, K. Honda, Nature 238 (1972) 37-38.
- [4] X. Chen, L. Liu, P.Y. Yu, S.S. Mao, Science, 331, 746-750, 2011.
- [5] B. Chai, T. Peng, P. Zeng, J. Mao, J. Mater. Chem., 21, 14587-14593, 2011.
- [6] S. Rengaraj, S. Venkataraj, C.W. Tai, Y. Kim, E. Repo, M. Sillanpää Langmuir, 27, 5534-5541, 2011.
- [7] X. An, J.C. Yu, F. Wang, C. Li, Y. Li, Appl. Catal. B: Environ., 129, 80-88, 2013.
- [8] H. Bai, Z. Liu, D.D. Sun, ChemPlusChem, 77, 941-948, 2012.
- [9] F. Ye, G. Du, Z. Jiang, Y. Zhong, X. Wang, Q. Cao, J.Z. Jiang, Nanoscale, 4, 7354-7357, 2012.
- [10] P. Gao, M.H. Tai, D.D. Sun, ChemPlusChem, 78, 1475-1482, 2013.